

Numerical Analysis of Unsteady Viscous Flow Through a Weis-Fogh Type Ship Propulsion Mechanism Using the Advanced Vortex Method

Ki-Deok Ro[†] · Myeong-Hun Kang* · Tae-Hee Kong*
(Manuscript : Received OCT 17, 2005 ; Revised NOV 21, 2005)

Abstract : The velocity and pressure fields of a ship's Weis-Fogh type propulsion mechanism are studied in this paper using an advanced vortex method. The wing (NACA0010 airfoil) and channel are approximated by source and vortex panels, and free vortices are introduced away from the body surfaces. The viscous diffusion of fluid is represented using the core-spreading model to the discrete vortices. The velocity is calculated on the basis of the generalized Biot-Savart law and the pressure field is calculated from an integral, based on the instantaneous velocity and vorticity distributions in the flow field. Two-dimensional unsteady viscous flow calculations of this propulsion mechanism are shown, and the calculated results agree qualitatively with the measured thrust and drag due to un-modeled large fluctuations in the measured data.

Key words : Computational fluid dynamics, Vortex method, Propulsion mechanism, Unsteady flow

1. Introduction

The Weis-Fogh mechanism, discovered through the analysis of wing motion in the hovering flight of a small bee called *Encarsia Formosa*, is a novel and very efficient mechanism for lift generation^{[1],[2]}. In the flight of this tiny bee, the beating rate of the wings is about 400Hz, and the Reynolds number R_e , defined by the wing chord and mean velocity of the leading edge, is approximately 30. However, the

lift coefficient value of C_L is approximately 3~4, even when including the cilium around the wing in the wing area, which is even higher than 1.6. This magnitude is much higher when comparing the lift of steady wings for such a low Reynolds number and this means that the insect efficiently generates lift^[1].

Tsutahara^{[3],[4]} presented the propulsion model, which used a two-dimensional model of the Weis-Fogh mechanism in the

[†] Corresponding Author (School of Mechanical and Aerospace Engineering, Institute of Marine Industry, Gyeongsang National University), E-mail : rokid@gaechuk.gsnu.ac.kr, Tel : 055)640-3123

* Graduate School, Department of Mechanical System Engineering, Gyeongsang National University

water channel, and showed that this propulsive device operates very effectively by conducting experiments on the dynamic characteristics, and a working test on a model ship as the new ship propulsion system. Ro^[5] simulated the unsteady flow fields by applying the conventional discrete vortex method on the circumference of the wing while the propulsive mechanism was being operated, and also verified the time variation of the thrust and the drag on the wing. Due to carrying out the simulation as potential flows without viscosity and a consideration of the wing as a plate without thickness, the numerical predictions have limitations compared with the experimental results.

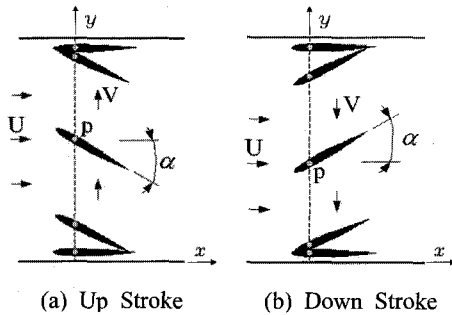


Fig. 1 A model of propulsion mechanism

This paper, therefore, clearly verifies the velocity and pressure fields in the Weis-Fogh-type ship propulsion mechanism using the advanced vortex method^[6], and contributes to its practical application as a propulsion system.

2. Numerical Method

2.1 A Model of a Propulsion Device

Fig. 1 shows the analytical model of a Weis-Fogh type ship propulsion

mechanism. Perpendicularly, the figure shows the upper part of the model, and, as a wing in the water channel oscillates in a reciprocal operation, the propulsive power rises to the left (the direction towards which the ship is progressing). This model is identical to the Tsutahara et al. model^[3], and so a brief synopsis of it will be sufficient.

A wing is installed in a square channel. When the point P corresponding to the center axis of the wing is oscillated back and forth along the y -axis, the wing first opens at point P from the lower surface (opening stage). Then, maintaining an open angle α , the wing moves translationally in a parallel movement (translating stage), and finally rotates and closes on the upper surface (closing stage) through the reciprocal motion of point p . It then executes an opening stage at the upper surface once more, moves translationally once again, and repeats the closing stage at the lower surface.

Originally, in the Weis-Fogh mechanism, circulation in the opposite direction is formed at each position of wing, as a pair of flat-plate wings open while their trailing edges touch. However, through the principle of a mirror image, when channel walls are placed and the same motions as above are executed by a single wing, as shown in the analytical model of Fig. 1, the identical effects can be achieved with a pair of wings.

2.2 Introduction of a nascent Vortex Element

The model of the Weis-Fogh type propulsion mechanism utilizes the driving

system shown in Fig. 1. Comparing it with the results of Ro's experiment^[5], the numerical model was found to have a hydrodynamic similarity with the experimental conditions, and the shape of the wing was also set at NACA0010, as given in the reference. By calculating the velocity and the pressure field of this propulsion unit during the movement of the wing shown in Fig. 1(a) and 1(b) for every time step, we could examine the results. The movement of the wing at the opening and closing stages is easily represented by combining the translating and rotating motions. Here, assuming that two flat plates and a wing in the flow field were installed, the surfaces of each object were represented with double panels, that is, with a finite number of source and vortex panels. At this time, the unknowns that should be determined at each time step were the source strength on the panel for M pieces and the circulation around the wing and two walls of the water channel. These unknowns were obtained using the Neumann condition in Eq. (1) at the center of the source panel for M pieces ($i=1,2,3\cdots M$), and the theorem of Kelvin in Eq. (2) for the circulation around each object, $\Gamma_b = \gamma_{bs} \cdot S_b$.

$$\left\{ \sum_{j=1}^M (\mathbf{u}^{sp} + \mathbf{u}^{vp})_j + \sum_{k=1}^N \mathbf{u}_k^{vo} + \mathbf{U} \right\} \cdot \mathbf{n}_i = \mathbf{u}_i \cdot \mathbf{n}_i \quad (1)$$

$$\Gamma_b + \sum_{k=1}^{N_b} \Gamma_b^{vo} k = 0 \quad (2)$$

Here \mathbf{u}^{sp} , \mathbf{u}^{vp} and \mathbf{u}^{vo} are the induced velocities that were deduced from

the source panels, the vortex panels, and the vortex elements introduced into the flow field \mathbf{U} and \mathbf{u}_i are the uniform flow and the velocity of the i -th control point:

\mathbf{n}_i is the unit vector of the vertical direction at the i point: γ_{bs} and S_b represent the circulation of the unit length for each object circumference and the length of the circumference: and Γ_{bk}^{vo} is the circulation of the vortex element that is emitted by each object. Here, assuming that γ_{bs} is constantly distributed around the object, it can be obtained from $\gamma_{bs} = \Gamma_b / S_b$, then \mathbf{u}^{vp} is calculated by γ_{bs} . In the case of the conventional vortex method, it was found to be numerically unstable because it became more of a condition than a needed unknown, to which we applied the Neumann condition and the theorem of Kelvin, which expressed only the source panels or the vortex panels in the object surface. In this paper, however, by considering double fold of the source and vortex panels, the above stated problem could be solved.

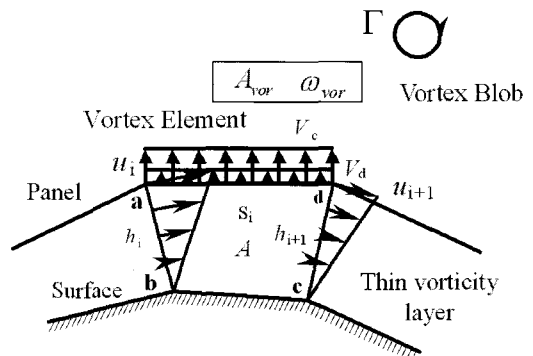


Fig. 2 Thin vorticity layer and nascent vortex element

Fig. 2 illustrates the schematic of the thin vorticity layer and the introductory method of the nascent vortex elements. The vorticity field near the solid surface is represented by the proper distribution of the vorticity layers and the discrete vortex elements to satisfy the non-slip condition on the body surface. A thin vorticity layer with thickness h_i was considered along the body surface, and the solid body was discretized by a number of source panels, as shown in Fig. 2. Assuming that the flow was considered two-dimensional and that there was a linear distribution of the velocity in the thin vorticity layer, and for the simplicity of illustration, suppose the solid is stationary, the normal convective velocity V_c on the outer boundary of the vorticity layer can be expressed using the relation of continuity of flow and the no-slip condition on the solid surface for the element of the vorticity layer [abcd] as

$$V_c = \frac{1}{s_i} \left\{ \frac{h_i u_i}{2} - \frac{h_{i+1} u_{i+1}}{2} \right\} \quad (3)$$

in which s_i , h_i and u_i represent the panel length, the thickness of the vorticity layer, and the tangential velocity at each node of outer boundary, respectively. As the solid is movable, Eq.(3) is still valid when u_i is thought of as a velocity relative to the moving solid. On the other hand, the vorticity of the thin shear layer diffused through the panel into the flow field. In order to consider this vorticity diffusion, we obtain the diffusion velocity V_d at the

outer boundary of the vorticity layer as

$$V_d = \frac{1.136^2 \nu}{h_i + h_{i+1}} \quad (4)$$

Here, ν is the kinematic viscosity of the fluid. If the value of $(V_c + V_d)$ becomes positive, a nascent vortex element is introduced in the flow field, where the thickness h_{vor} and the vorticity ω_{vor} of the vortex element are obtained as follows:

$$h_{vor} = (V_c + V_d) dt \quad (5)$$

and

$$\omega_{vor} = \frac{\Gamma}{A + A_{vor}} \quad (6)$$

Here, Γ is the circulation originally involved in the element of the vorticity layer [abcd] calculated according to Eqs.(1) and (2), and A and A_{vor} are the areas of the vorticity layer element and the nascent vortex element. The square-type vortex element generated during each time step is substituted with a vortex blob at a fixed height. Moreover, as a linear distribution of velocity is assumed in the thin vorticity layer, the shearing stress on the wall surface is evaluated approximately from the following equation, as long as the thickness of the vorticity layer is sufficiently thin:

$$\tau_w = \mu \frac{\partial u}{\partial y} = -\mu \omega \quad (7)$$

2.3 Calculation of the Velocity Field

A trajectory of the vortex shedding element over the time step dt is approximately written by applying the following Adams-Bashforth method as:

$$\mathbf{r}(t+dt) = \mathbf{r}(t) + \{1.5\mathbf{u}(t) - 0.5\mathbf{u}(t-dt)\}dt \quad (8)$$

in which the motion \mathbf{u} of the vortex element can be derived from the following Biot-Savart law (9) that includes source panels, vortex sheet panels and all vortex elements existing in the flow field.

$$\mathbf{u}(\mathbf{r}) = \frac{1}{2\pi} \int_V \frac{\boldsymbol{\omega} \times \mathbf{R}}{R^2} dV - \frac{1}{2\pi} \times \int_{S_0} \left[\frac{(\mathbf{n}_0 \cdot \mathbf{u}_0) \cdot \mathbf{R}_0}{R_0^2} - \frac{(\mathbf{n}_0 \times \mathbf{u}_0) \times \mathbf{R}_0}{R_0^2} \right] dS_0 \quad (9)$$

In the second term of the RHS in Eq.(9), \mathbf{R}_0 represents $\mathbf{R}_0 = \mathbf{r} - \mathbf{r}_0$ and $R_0 = |\mathbf{R}_0|$.

The Lagrangian expression for the vorticity transport equation is expressed as:

$$\frac{d\boldsymbol{\omega}}{dt} = (\boldsymbol{\omega} \cdot \text{grad})\mathbf{u} + \nu \nabla^2 \boldsymbol{\omega} \quad (10)$$

in which, in a two-dimensional case, the first term of the RHS disappears, and in the second term, the viscous diffusion term remains. This viscous diffusion term is approximated using the core spreading method^[7].

$$\varepsilon_k(t+dt) = \varepsilon_k(t) + \frac{2.242^2 \nu}{2\varepsilon_k(t)} dt \quad (11)$$

According to Eq. (9), in the flow fields of this propulsion mechanism, the vortex

distribution, streak line and velocity field are predicted in each time step, and the streamline are plotted from the vector field.

2.4 Calculation of the Pressure Field

If the divergence is applied to the Navier-Stokes equation, the pressure Poisson equation becomes:

$$\nabla^2 p = -\rho \text{div}(\mathbf{u} \cdot \text{grad} \mathbf{u}) \quad (12)$$

In general, the pressure field is obtained by calculating the Poisson equation using the finite difference method. In this case, some lattices must be generated in the flow field, such that the merits of the vortex method that the grid generation does not need would be lost. Therefore, in this research, instead of using the finite difference method of the Poisson equation, the pressure in the flow field is obtained from the integration equation formulated by Uhlman^[8], as follows:

$$\beta H + \int_{S_0} H \frac{\partial G}{\partial \mathbf{n}} dS_0 = - \int_V \nabla(\mathbf{u} \times \boldsymbol{\omega}) dV - \int_{S_0} \left\{ G \cdot \mathbf{n} \cdot \frac{\partial \mathbf{u}}{\partial t} + \nu \cdot \mathbf{n} \cdot (\nabla G \times \boldsymbol{\omega}) \right\} dS_0 \quad (13)$$

in which $\beta = 1$ refers to the inside flow and the boundary surface S_0 is represented by $\beta = 1/2$. G is the fundamental solution of the scalar Laplace equation with the delta function expressed as:

$$G = \frac{1}{2\pi} \log\left(\frac{1}{R}\right) \quad (14)$$

and H is the Bernoulli-type variable, defined as follows:

$$H_i = \frac{p_i}{\rho} + \frac{u_i^2}{2} \quad (15)$$

The pressure field of the propulsion mechanism was calculated from the pressure distribution on the body surfaces using Eqs. (13) and (15) during each time step, and with this information, isobaric lines of the entire flow field were taken. By integrating the normal component of the pressure and the tangential component of the shear stress around the wing surface, the hydrodynamic force F acting on the wing was obtained simply using:

$$F = iF_x + jF_y = \oint_{S_0} \{(-p \cdot n) + \tau_w \cdot t\} dS_0 \quad (16)$$

in which F_x and F_y represent the components of force at the x and y directions, taken as the thrust T and the drag force D for the negative direction. That is, the thrust and the drag forces on the wing at each time step are calculated using Eq. (16).

2.5 The Calculation Conditions

To easily compare the experimental results, the same calculation conditions were given as set in the experiment conditions of the visualization by Ro^[5]. That is, the wing chord is set as $C=1$, uniform flow is $U=1$, movement velocity of the wing axis is $V=1$, the attack angle of the wing is $\alpha=30^\circ$, the distance from the trailing edge of the wing to the

wing axis r_p is $r_p=0.75C$, and the length, width and thickness of the water channel are $l=5.75C$, $h=2.5C$ and $0.02C$ respectively. Tsutahara et al^[3] showed experimentally a higher thrust efficiency at the velocity ratio $V/U=1.0$ with the angle of attack $\alpha=30^\circ$.

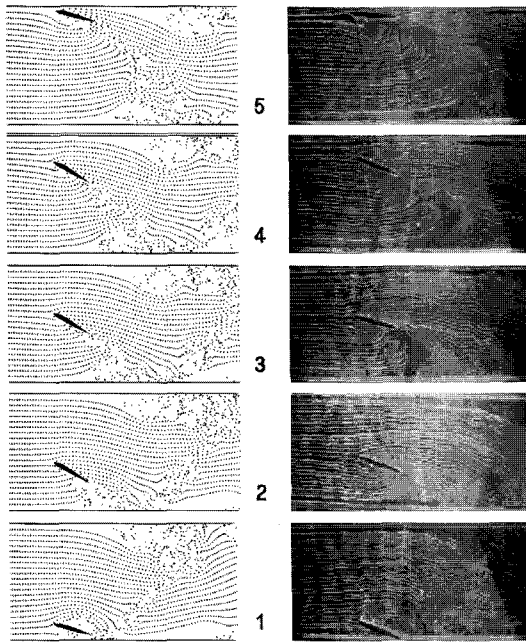
As expressed in the previous section, it was assumed that two flat plates and a wing in the flow field were installed, the surfaces of each object were represented with double panels, that is, with a finite number (M_b pieces) of source and vortex panels, where the panels of each object are $M_b=80$.

In the present calculation, the time step size dt was set at $dt=0.015$ during the translating stage and as $dt_o=dt \times r_p C$ and $dt_c=dt \times (1-r_p)C$ during the opening and closing stages. The results of the above procedure reveal the values for the time steps where the distances moved by the leading or trailing edges are all equal during the entire stroke.

3. Results and Discussion

Fig. 3 shows the continuous flow pattern around the wing (NACA0010) during one stroke for $Re=5900$, the Reynolds number Re as defined by the wing chord and uniform flow. In Fig. 3, (a) refers to the numerical results of the streak lines and (b) represents the visualization photograph observed in the hydrogen bubble technique by Ro^[5] under the same conditions as in Fig. 3 (a). In Fig. 3, 1 represents the opening stage; 2 to 4, the translating stage; and 5, the

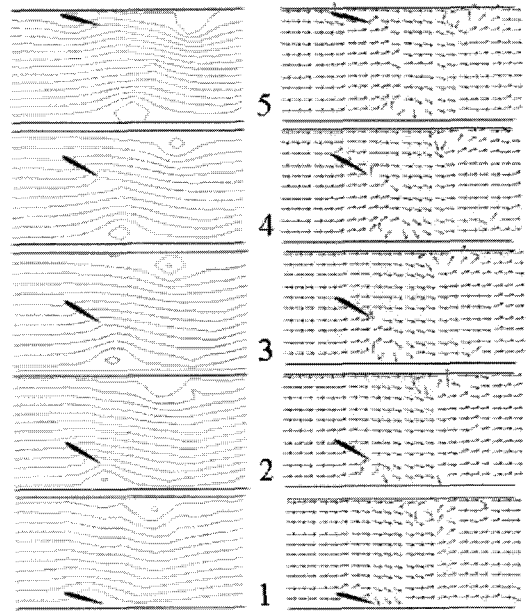
closing stage. The discontinuity of the streak lines seen in the vicinity of the trailing edge is due to the effects of the vortices generated at the trailing edge. Overall, the simulation results of the entire stage match the visualized picture.



(a) Simulation (b) Photograph
Fig. 3 Streak lines for one stroke of the wing
 ($C=1$, $h=2.5C$, $V/U=1.0$, $r_p=0.75C$ and $\alpha=30^\circ$)

Fig. 4 shows the streamlines (a) and the velocity vectors (b) around the wing during one stroke, under the same conditions as in Fig. 3. Here, considering the streamlines that passed the wing, we know that the flow goes around the wing, because streamlines bend to the moving direction of the wing at all stages and move together with the wing. The streamlines on the closed curve near both sides of the water channel were the effect of the vortex due to the occurrence of the

reciprocating motion in the wing. As shown in the velocity vectors (b), the clockwise vortex existed at around the lower part of the wall, while the counterclockwise vortex appeared near the upper part of the wall.



(a) Streamlines (b) Velocity vectors
Fig. 4 Flow patterns for one stroke of the wing

Fig. 5 shows the distribution of the pressure coefficient C_p on the surface of the wing. In Fig. 5, (a), (b) and (c) represent the opening, translating and closing stages, respectively. These correspond to positions 1, 3 and 5 in Figs. 3 and 4. Moreover, 0.0 point in the horizontal axis for each figure corresponds to the p point in Fig. 1 and to the distance $r_p=0.75C$ from the trailing edge to the p point. The arrows show the directions of the pressure distribution, which moved in a counterclockwise direction starting from

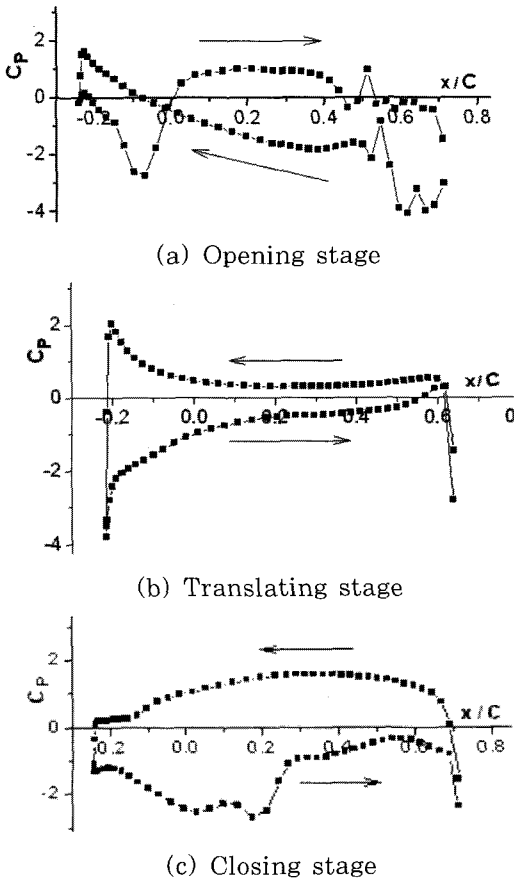


Fig. 5 Pressure distribution around the wing ((a),(b) and (c) on the figure correspond to the points 1, 3 and 5 on Fig. 3)

the trailing edge of the wing. Considering the pressure distribution at the opening stage (a), the pressure coefficient in the backside for the uniform flow had a negative value from the trailing edge to the p point (the 0.0 point), while the pressure on the pressure side indicated almost a positive value except at the vicinity of the trailing edge. Contrarily, the pressure on the backside for the uniform flow had an almost negative value from the P point to the leading edge but showed a positive value on the pressure side. Considering the pressure

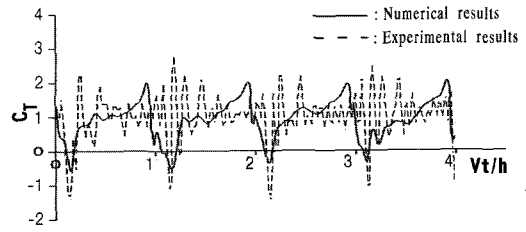


Fig. 6 Time variations for thrust coefficients

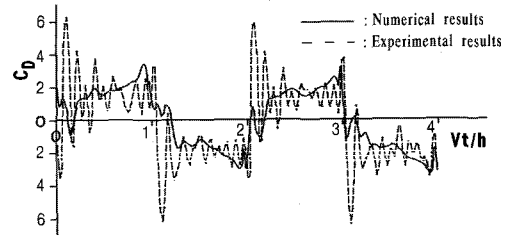


Fig. 7 Time variations for drag coefficients

distribution around the wing at the translating stage (b), the pressure coefficient in the backside value for the uniform flow was almost positive, while the pressure on the pressure side showed a negative value. More significantly, it was also proven that the pressure difference between the pressure side and the backside appeared in the vicinity of the leading edge. Considering the pressure distribution at the closing stage (c), the pressure coefficient in the backside for the uniform flow had a positive value similar to that in the translating stage, while the pressure on the pressure plane had a negative value even as the pressure difference between the pressure side and the backside was not significant at the vicinity of the leading edge.

Fig. 6 shows the time history of the thrust coefficient C_T at $\alpha = 30^\circ$ and $V/U = 1.0$. The horizontal axis in the figure represents the value that the

moved distance of the wing axis is divided by the channel width. This value corresponds to the number of strokes. In Fig. 6 the solid lines represent the numerical results using this calculating method while the dashed lines are the experimental results were measured by $Ro^{[5]}$ under the same conditions. The reason that the experimental results have the large fluctuations is due to the surface wave generated by the movement of the wing, and particularly the larger fluctuations occurred in the early stage of each stroke is because the wing axis is instantaneously acted at the large force, due to the inertial force of the wing and the flow around the wing. In the opening stage, the thrust coefficient C_T shows a negative value for both the numerical and experimental results while in the translating stage, the numerical results show an increase as time passes. This trend is not analyzable from the experimental results due to severe fluctuation.

Fig. 7 shows the numerical and experimental results of the drag coefficient C_D taken in the same conditions as in Fig. 6. The drag coefficient C_D also showed a fairly good match in the qualitative trend between the calculated and measured results. The drag coefficient C_D also gradually increased as the wing approaches the opposite wall, in which it started from a wall, though the experimental results can be undistinguishable due to the large fluctuations. The mean values of thrust coefficient and the drag coefficient were approximately 1.0 and 2.0 respectively at

both the solid and the dashed lines of Figs. 6 and 7 and the numerical results were also quantitatively compatible with the experimental results.

In Figs. 6 and 7 the reason why the numerical results (solid lines) do not coincide with the experimental results (dashed lines), except the large fluctuations described the above, is considered that in the analytical model of Fig. 1 the flow surrounding the wing was assumed as 2-dimensional while in the actual experiment the free surface above the wing would affect the flow around the wing making it not thoroughly 2-dimensional.

4. Conclusions

This research simulated the velocity and pressure fields of a Weis-Fogh type ship propulsion mechanism using the advanced vortex method. The wing and water channel were presented through a finite number of source and vortex panels, and the vortex shedding was taken from the entire surface of each object. Both the velocity and the pressure field were evaluated with integral equations. The streak lines were shown to coincide with the visualization picture. The analyzed results are summarized as follows:

(1) The vortices that were in the opposite direction of each other near both walls of the water channel were generated along the reciprocating motion of the wing.

(2) The pressure distribution on the wing surface was shown to have entirely

different characteristics during the opening stage, the translating stage and the closing stage.

(3) The coefficients of the thrust C_T and the drag C_D gradually increased as the wing approaches the opposite wall, in which it started from a wall.

Acknowledgments

This work was supported by the Korea Research Foundation Grant (KRF-2003-041-D00639) and the NURI Project, in which the main calculations were performed by using the supercomputing resources of the Korea Institute of Science and Technology Information (KISTI).

References

- [1] Weis-Fogh, T., "Quick Estimates of Flight Fitness in Hovering Animals, Including Novel Mechanism for Lift Production", *J. Exp. Bio.* Vol. 59, pp. 169-230, 1973.
- [2] Lighthill, M. J., "On the Weis-Fogh Mechanism of Lift Generation", *J. Fluid Mech.* Vol. 60, pp. 1-17, 1973.
- [3] Tsutahara, M. & Kimura, T., "An Application of the Weis-Fogh Mechanism to Ship Propulsion", *Trans. ASME J. Fluids Eng.* Vol. 109, No. 2, pp. 107-113, 1987.
- [4] Tsutahara, M., Kimura, T. & Ro, K. D., "Ship Propulsion Using the Weis-Fogh mechanism", *Bull. Mari. Eng. Soc. (in Japan)*. Vol. 17, No. 2, pp. 49-55, 1989.
- [5] Ro, K. D., "Calculation of Thrust and Drag Characteristics for Ship's Propulsion Mechanism of Weis-Fogh Type", *KSME Intl. J.*, Vol. 14, No. 11, pp. 1249-1258, 2000.
- [6] Kamemoto, K., "On Attractive Features of the Vortex Methods", *Comp. Fluid Dyn. Rev.* 1995 ed. Hafez, M. & Oshima, K. JOHN WILEY & SONS., pp. 334-353.
- [7] Leonard, A., "Vortex Methods For Flow Simulations", *J. Comp. Phys.*, Vol. 37, pp. 289-335, 1980.
- [8] Uhlman, J. S., "An Integral Equation Formulation of the Equation of Motion of an Incompressible Fluid", *Naval Undersea Warfare Center T.R.*, pp. 10-086, 1992.

Author Profile



Ki-Deok Ro

Date of birth : June 16, 1953.

Pukyong National University, 1973 to 1977, Bachelor of Marine Engineering. Kobe University, 1984 to 1986, Master of Mechanical Engineering. Kobe University, 1986 to 1989, Doctor of Mechanical Engineering. Mobil oil Company, 1977 to 1979, Marine Engineer. National Tongyeong Fisheries College, 1979 to 1995, Professor. Gyeongsang National University, 1995 to present, Professor.



Myeong-Hun Kang

Date of birth : May 26, 1977.

Gyeongsang National University, 1996 to 2004, Bachelor of Marine Engineering. Graduate School of Gyeongsang National University, 2004 to present, Master course student.



Tae-Hee Kong

Date of birth : July 29, 1953.

Pukyong National University, 1973 to 1977, Bachelor of Marine Engineering. Pukyong National University, 1991 to 1993, Master of Marine Engineering. Pukyong National University, Graduate School of Gyeongsang National University, 2004 to present. Doctor course student.